Living Donor-Recipient Pair Matching for Liver Transplant via Ternary Tree Representation With Cascade Incremental Learning

Anam Nazir, Muhammad Nadeem Cheema, Bin Sheng, *Member, IEEE*, Ping Li, *Member, IEEE*, Jinman Kim, *Member, IEEE*, and Tong-Yee Lee, *Senior Member, IEEE*

***Abstract*—Visual understanding of liver vessels anatomy between the living donor-recipient (LDR) pair can assist surgeons to optimize transplant planning by avoiding non-targeted arteries which can cause severe complications. We propose to visually analyze the anatomical variants of the liver vessels anatomy to maximize similarity for finding a suitable Living Donor-Recipient (LDR) pair. Liver vessels are segmented from computed tomography angiography (CTA) volumes by employing a cascade incremental learning (CIL) model. Our CIL architecture is able to find optimal solutions, which we use to update the model with liver vessel CTA images. A novel ternary tree based algorithm is proposed to map all the possible liver vessel variants into their respective tree topologies. The tree topologies of the recipient's and donor's liver vessels are then used for an appropriate matching. The proposed algorithm utilizes a set of defined vessel tree variants which are updated to maintain the maximum matching options by leveraging the accurate segmentation results of the vessels derived from the incremental learning ability of the CIL. We introduce a novel concept of in-order digital string based comparison to match the geometry of two anatomically varied trees. Experiments through visual illustrations and quantitative analysis demonstrated the effectiveness of our approach compared to state-of-the-art.**

***Index Terms*—Image enhancement, computed tomography angiography, incremental learning, liver transplantation, liver variants, ternary tree representation, vessels segmentation.**

I. Introduction

LIVER transplantation is a well-known surgical procedure to treat patients having end-stage liver diseases which can result in a considerable increase in life expectancy. In this surgery, the knowledge of the liver vasculature system is essential to distinguish variations in living donor-recipient (LDR) vascular anatomy for avoiding eventual complications regarding vessels anomalies such as portal and hepatic veins thrombosis [1], [2]. For living donor, surgeons need to ensure that the relative residual liver volume (RLV) is large enough and the remnant liver has adequate blood supply from both hepatic and portal venous systems when grafting liver parts. Preoperative computed tomography angiography (CTA) volumes provide a non-invasive evaluation approach to identify liver composition, pathology, and to identify suitable donors; however, this is currently a complex manual procedure [3]–[9]. This research aims to quantify and maximize the availability of anatomical variants of liver vasculature system, segmented from CTA volumes, and use it to compare a specific recipient with available potential donor's liver transplantation. There is a novel clinical motivation of this study which is to provide surgeons with a comprehensive pre-operative evaluation [10] of the liver vascular system to understand the variations of living donor-recipient (LDR) vascular anatomy [11]. This evaluation can reduce the risks to the donors, e.g. toxic exposure of the liver parenchyma, and maximize benefits to the recipient, e.g. to avoid non-optimal pairing (recipient rejection) [12], [13].

In the past few years, deep convolutional neural networks (CNN) have become the state-of-the-art in regards to liver vessel segmentation [14], [15]. These networks can instinctively discover compound image attributes and merge them into hierarchical abstraction for classification and segmentation. On the other hand, a large number of connecting parameters in filters and layers leads deep structures to require time-consuming and data intensive model training. Moreover, a deep model may experience insufficient features to represent the input data [16], [17]. A conventional solution to address these limitations is to add new features by mounting the number of filters or layers

Manuscript received July 28, 2020; revised November 4, 2020 and December 16, 2020; accepted January 5, 2021. Date of publication January 8, 2021; date of current version July 19, 2021. This work was supported in part by the National Natural Science Foundation of China under Grants 61872241 and 61572316, in part by The Hong Kong Polytechnic University under Grants P0030419 and P0030929, and in part by the Ministry of Science and Technology, Taiwan under Grant 108-2221-E-006-038-MY3. *(Corresponding author: Bin Sheng.)*

Anam Nazir is with the Department of Computer Science and Engineering, Shanghai Jiao Tong University.

Muhammad Nadeem Cheema is with the Department of Computer Science and Engineering, Shanghai Jiao Tong University, and also with the Department of Computer Science, COMSATS University Islamabad Islamabad.

Bin Sheng is with the Department of Computer Science and Engineering, Shanghai Jiao Tong University, Shanghai 200240, China (e-mail: shengbin@sjtu.edu.cn).

Ping Li is with the Department of Computing, The Hong Kong Polytechnic University.

Jinman Kim is with the Biomedical and Multimedia Information Technology Research Group, School of Information Technologies, The University of Sydney.

Tong-Yee Lee is with the Department of Computer Science and Information Engineering, National Cheng-Kung University.

Digital Object Identifier 10.1109/TBME.2021.3050310

0018-9294 © 2021 IEEE. Personal use is permitted, but republication/redistribution requires IEEE permission.
See https://www.ieee.org/publications/rights/index.html for more information.

Authorized licensed use limited to: National Cheng Kung Univ.. Downloaded on July 20,2021 at 04:15:33 UTC from IEEE Xplore. Restrictions apply.

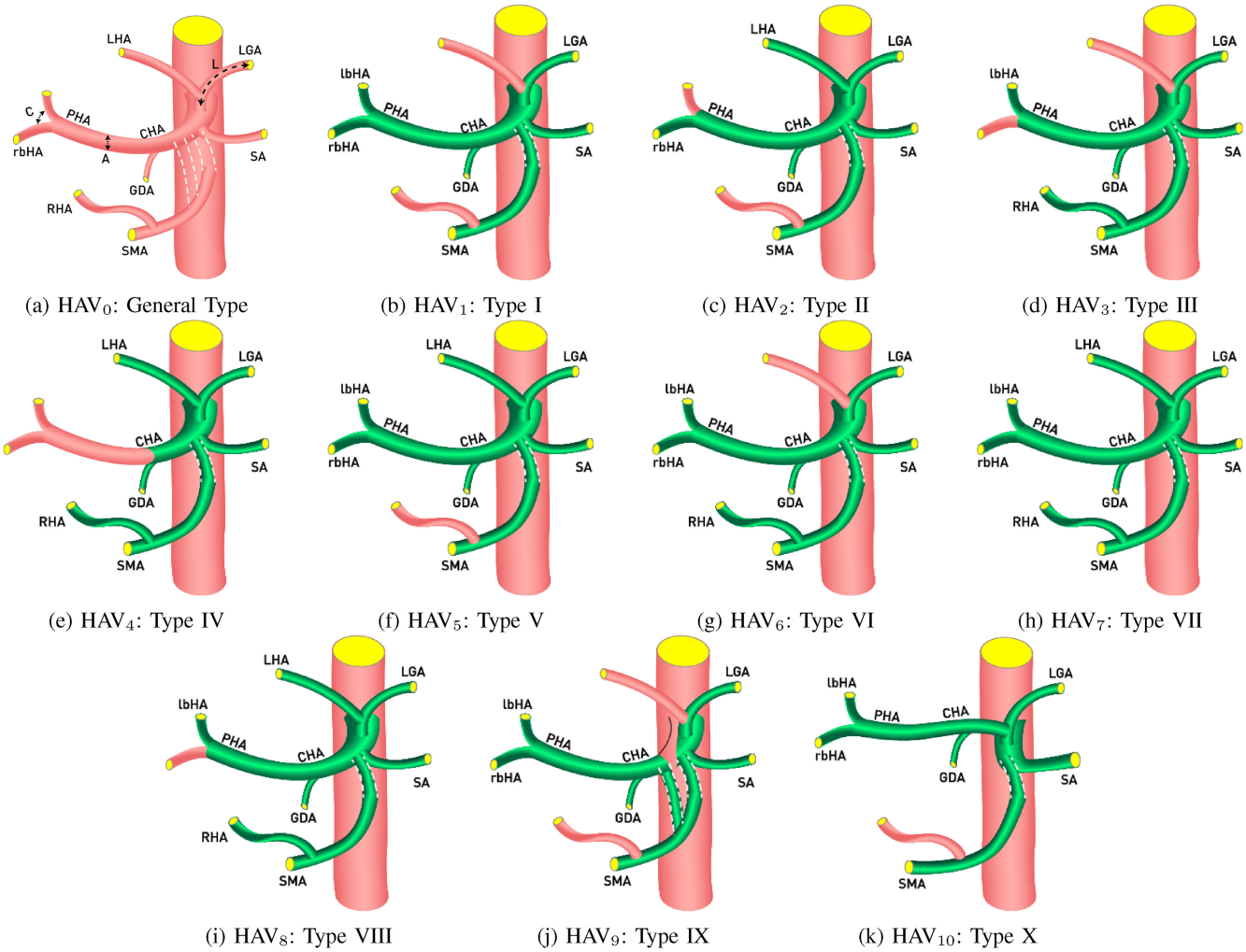

(a) HAV_0: General Type (b) HAV_1: Type I (c) HAV_2: Type II (d) HAV_3: Type III

(e) HAV_4: Type IV (f) HAV_5: Type V (g) HAV_6: Type VI (h) HAV_7: Type VII

(i) HAV_8: Type VIII (j) HAV_9: Type IX (k) HAV_{10}: Type X

Fig. 1. Detailed anatomical variants of hepatic artery based on Michel's classification [20] from HAV_0 to HAV_{10}. (a) First one is the general type representing all variants, (b) Type I is conventional type for which the common hepatic artery (CPA), starting from the celiac artery (CA) splits into the right hepatic artery (RHA) and left hepatic artery (LHA) followed by the proper hepatic artery (PHA), (c) In type II, LHA originating from the left gastric artery (LGA) feeding the left liver, and a middle hepatic artery (MHA) feeding the right liver, (d) In type III, RHA is originating from superior mesenteric artery (SMA), feeds the right liver, and a MHA feeds the left liver, (e) Type IV corresponds to the connection of type II and III variants, with the presence of a RHA for the right liver and a LHA feeding the left liver, (f) Type V expresses the presence of a LHA originating from the LGA in addition to the left branch of the hepatic artery, (g) Type VI connects the RHA starting from the SMA and the right branch of the hepatic artery, (h) Type VII associates variants V and VI which delivers combination of PHA with the right and left branch + RHA staring from the SMA + LHA originating from the LGA, (i) In type VIII right liver is only fed by the RHA, while there is dual vessels supply of the left liver via the MHA and LHA, (j) In type IX the CHA originates from the SMA, and (k) In type X the CHA originates from LGA.

and then retrain the whole model from the start, which may prove to be a time-consuming process, especially for the deep architectures [18], [19].

In the liver transplantation scenario, the training data, in the form of a donor CTA volume, is being updated to find an appropriate match between LDR livers, so the trained model needs to be adapted for the new data. The limitation of using the deep network to segment liver vessels is the requirement of retraining the entire model with all the training data to accommodate the newly received input [16]. On the contrary, the recent concept of cascade incremental learning (CIL) through broad learning system (BLS) [21] can be well tailored to the new training data by updating the related part of the network weights for the additional input data (donor CTA volumes). To alleviate the problem of CNN for sustaining its accessibility to add available donor variants for an appropriate match and extract more features without retraining the whole system for liver vessels segmentation process, we have introduced cascade incremental learning as a flat network model. In the proposed architecture, the input CTA volumes are divided into possible feature nodes of available donor tree variants (hepatic artery and portal vein varaints, see Fig. 1 and Fig. 2) for an appropriate match and the designed model is extended in a flat way with enhancement nodes using incremental learning concept for a new input arriving.

Several approaches have been introduced to model the segmented liver vascular systems through iteratively labelling each of the vessel branches according to its relationships with its neighbouring labelled branches using top-down or backward tracking scheme. However, all of these approaches are based

Authorized licensed use limited to: National Cheng Kung Univ.. Downloaded on July 20,2021 at 04:15:33 UTC from IEEE Xplore. Restrictions apply.

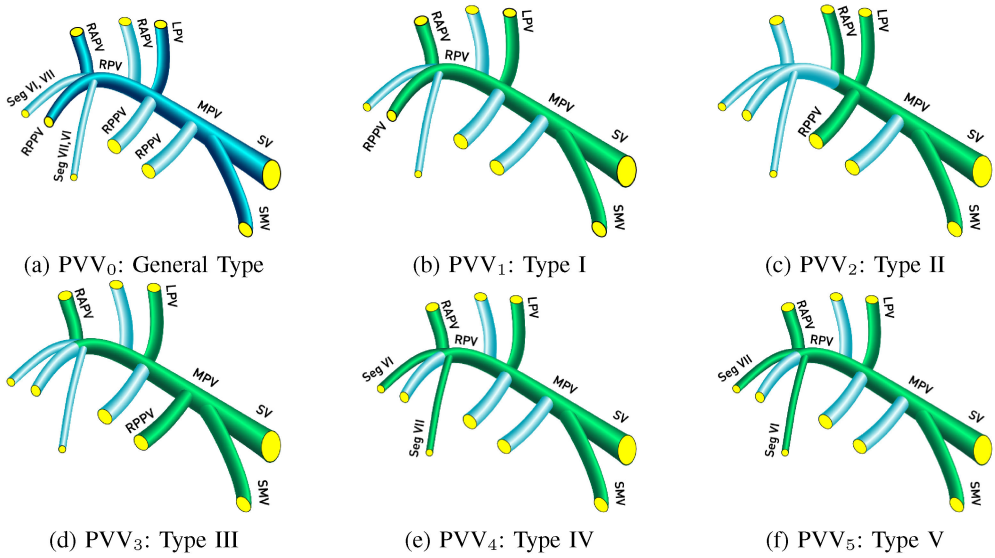

Fig. 2. Detailed anatomical variants of portal vein from PVV_0 to PVV_5. (a) First one is the general type representing all variants of portal vein, (b) Type I is classical anatomy, (b) Type II represents trifurcation in portal vein, (c) Type III depicts right posterior vein as first branch of main portal vein (MPV), (d) Type IV involves seg VII as a separate branch of right portal vein (RPV), and (e) Type V indicates seg VI as separate branch of RPV.

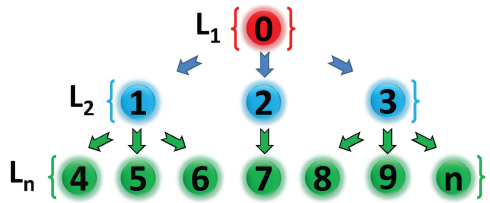

Fig. 3. General representation of ternary tree with respect to levels (L_1 to L_n).

on local relationships of the branches. Apart from these methods, there exist other approaches for portal and venous tree separation. Yan *et al.* [1] proposed a method to model the liver vessels by employing Twin-Line RANSAC and Murray's Law. In another study [22], they used an edge-based structure for liver venous tree separation. Aylward *et al.* [23] proposed an algorithm with tree notation to register an image for liver vasculature analysis. However, liver vessels tree matching problem for transplantation procedure is more precise than tree separation as liver vasculature of LDR may be anatomically different [22]. Hence, the matching process of two geometrically varied tree structures implies pruning of both trees for covering all possible variants of available donors for the respective recipient.

In this research, we initially segment the liver vessels structures from the CTA for both the donor and the recipient using CIL, inspired from the recent work on liver venous tree separation [1], [24]. We compare the anatomy of recipient liver vasculature with available donor candidate's variants to find a suitable pair based on the ternary tree representation, see Fig. 3. Motivation to use the ternary tree for comparing the geometry of two anatomically varied trees is the convenient mapping of liver vasculature to its respective tree shapes. Moreover, the trees may prove to be a well-known representation of liver vascular systems segmented from CTA volumes. The tree nodes represent bifurcations/trifurcations (the dividing parts) and edges correspond to vessels between the nodes. We have employed in-order traversing for particularly comparing two anatomically varied tree structures. Our possible variants of liver vessels trees are identical from the root and varied at the leaf levels. Therefore, in-order traversing [25] proved to be an intelligent searching, as it will eliminate those donor tree variants which are not appropriate for the candidate recipient at the start of matching process (at leaf nodes). For experimental analysis, we have calculated the success and failure rates based on CAL (connectivity, area, and length of branches) score for each variant to compare the topological variations between two liver variants at concrete level. Following are the key contributions of our proposed method:

- **Liver Vessel Segmentation:** We leverage the incremental learning in a cascade feature mapping way by updating the input CTA training model to optimize the segmentation capability.
- **Tree Mapping:** We introduce a novel ternary tree based matching algorithm to map topologically varied liver vessels structures for better visualization of their respective tree representation.
- **Digital String Based Matching:** Our ternary tree in-order traversing is designed to efficiently compare the digital strings of two anatomically varied vessel structures to find a suitable match between the given recipient data against the possible donor variants.
- **Performance Analysis:** We quantified the similarity in terms of success and failure rates for vascular trees using strahler ordering metric. In according to the above three advantages, our method can compute very efficiently for finer visualization of liver tree structures which can increase chances for the successful LDR pair matching.

Authorized licensed use limited to: National Cheng Kung Univ.. Downloaded on July 20,2021 at 04:15:33 UTC from IEEE Xplore. Restrictions apply.

II. Related Work

A. Methods to Segment Liver Vessels Structure

Deep CNN is the state-of-the-art in segmentation of liver vessels structures [26]–[28]. Deep networks can intuitively ascertain multi-part image attributes and combine them into a hierarchical generalization for segmentation and classification. However, existing CNN techniques are primarily suitable for datasets having fewer variety in input images. In reality, when the dataset has a lesser amount of changeability, machine learning techniques are suitable for attaining voxel level classification which escorts to speedy CNN training and converging [29]. Especially, for cases like liver transplantation, where the training data in the form of donor CTA volume is being updated, the constructed model should be adaptive for new data to cope with the problem of insufficient features for required output [16]. One possible solution for above-mentioned problems is to extract more new features by growing the number of filters/layers and retrain the whole models from the start, which is a time-consuming and computationally expansive process [30]. BLS techniques have been recently used for image recognition [30], time series predictions [31], and classification problem [18]. Inspired by the advantages delivered by BLS, in this paper, our research introduced a novel method to leverage incremental learning in cascade manner for segmenting liver vessels structure robustly and efficiently.

B. Techniques to Represent and Compare Segmented Liver Vasculatures

Numerous techniques have been proposed to model/register the segmented vascular systems as a tree for visualization and follow-up for surgery planning in medical imaging. Few efforts modelled segmented skeletons and veins in graphs notations [22]. Other uses coherent point drift (CPD) approach in their algorithms to register a vascular system with an image [32]. Zhai *et al.* [33] use the Gaussian Mixture Model (GMM) to preserve the local tree topology for pulmonary vascular tree matching to quantifying morphological changes. A tree matching algorithm for intra-patient liver vessels registration is proposed in [34] to estimate liver deformation [35]. An algorithmic concept for quantifying measured vascular tree to model liver blood flow is provided in [36]. Moriconi *et al.* [12] have used minimum spanning tree to map and model retinal and cerebrovascular topologies. Another paradigm for liver venous tree separation have employed Twin-Line RANSAC with Murray's law [1] and edge-based structure [22]. Numerous efficient methods have been proposed [36] for detailed analysis of the patient's intra-hepatic vasculature in the form of 3D models of the liver vessels using CT volumes. However, there is still a research gap to provide surgeons a concrete and robust method to map and compare segmented liver vessels having geometrically varied alternatives to find a suitable match between LDR pair.

Ivashechenko *et al.* [37] designed a workflow to reduce the incidence of intraoperative biliary duct damage due to an unanticipated variation in the anatomy from MRI images. Guo *et al.* [38] proposed an automatic segmentation method of liver vessels based on graph cut, thinning, and vascular combination to obtain a complete liver vascular network.

For the liver transplantation procedure, a careful morphological investigation of vessel systems with branching pattern of all possible variants is a crucial precondition. Compared with related work, the advantages of this research is to provide a favourable method to robustly and accurately segment varied liver vessels structures using CIL. Also, to compare the anatomy of recipient liver vasculature with available donor candidate's variants for finding a suitable pair based on a novel usage of ternary trees.

III. Method

Fig. 4 shows the workflow of our approach having three major steps: (1) Liver vessels segmentation using CTA volumes as an input to the CIL model; (2) The segmented vessels are then mapped to a tree representation based on a well-known possible hepatic artery and portal vein variants and, (3) The tree matching step compares the recipient tree with the possible available donor tree variants to find an appropriate match. A detailed description of each module is discussed in the following subsections.

A. Liver Vasculature Segmentation Using Incremental Learning

Motivation to introduce CIL for segmenting liver vessels is that we may suffer from insufficient features from CTA volumes to cover all variants of liver vessels structures which may not well represent the valid LDR pairs. CIL's incremental ability can overcome this limitation. Motivated from original CIL, we propose new segmentation using incremental learning in a cascade manner as shown in below mentioned equations. A set of input CTA volumes I is divided into a collection of feature mapping nodes $S_1, S_2, \ldots, S_n$. For our setup, the first part of feature mapping nodes S_1 with mapping function ϕ is computed as:

$$S_1 = \phi(IX_{e1} + \alpha_{e1}) \triangleq \phi(I; \{X_{e1}, \alpha_{e1}\}) \tag{1}$$

Here X_{e1} and α_{e1} are arbitrarily produced weights and bias terms. Similarly, second group of feature nodes S_2 are calculated using the output of the S_1 nodes, so S_2 is articulated as:

$$\begin{aligned} S_2 &= \phi(S_1 X_{e2} + \alpha_{e2}) \\ &= \phi(\phi(IX_{e1} + \alpha_{e1})X_{e2} + \alpha_{e2}) \\ &\triangleq \phi^2(I; \{X_{ei}, \alpha_{ei}\}_{i=1,2}) \end{aligned} \tag{2}$$

In the same way we can compute all the n groups of input nodes as follows:

$$\begin{aligned} S_l &= \phi(S_{l-1} X_{el} + \alpha_{el}) \\ &= \phi^l(I; \{X_{el}, \alpha_{el}\}_{i=1}^{l}), for\ \ l = 1, \ldots, n; \end{aligned} \tag{3}$$

Here X_{el} and α_{el} are arbitrarily generated. Next, the determined feature nodes $S_n \triangleq [S_1, .., S_n]$ are associated with the enhancement nodes $\{E_m\}_{m=1}^{k}$,

$$E_m \triangleq \epsilon(S^n X_{Em} + \alpha_{Em}) \tag{4}$$

Authorized licensed use limited to: National Cheng Kung Univ.. Downloaded on July 20,2021 at 04:15:33 UTC from IEEE Xplore. Restrictions apply.

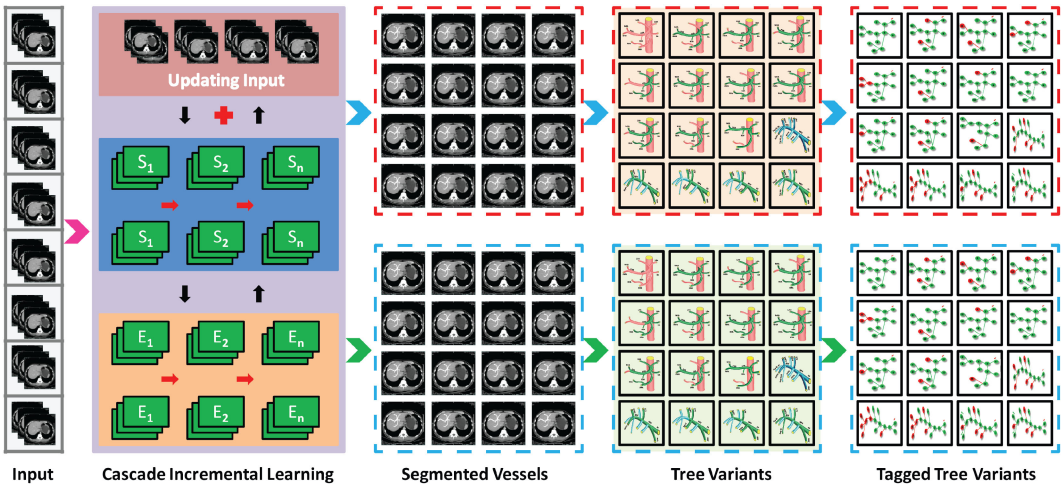

Fig. 4. The workflow of proposed model.

For feature nodes S^n and enhancement nodes E^m, the proposed CIL model is summarized as follows:

$$\begin{aligned} O &= [\phi(I;\{X_{e1},\alpha_{e1}\}),\ldots,\phi^n(I;\{X_{ei},\alpha_{ei}\}_{i=1}^n) \\ &\quad |\epsilon(S^nX_{E1}+\alpha_{E1}),\ldots,\epsilon(S^nX_{Em}+\alpha_{Em})]X_n^m \\ &= [S_1,\ldots,S_n|E_1,\ldots,E_m]X_n^m \\ &= [S^n|E^m]X_n^m \end{aligned} \tag{5}$$

Where $E_m \triangleq [E_1,...,E_m]$, and X_n^m are calculated through the pseudo-inverse of $[S^n|E^m]$. To formulate the incremental model of cascade network following computation is carried out. First, suppose if the (n + 1)th set of combined feature nodes is incrementally added and termed as $S^{(n+1)}$.

$$S_{n+1} \triangleq \phi^{n+1}(I;\{X_{ei},\alpha_{ei}\}_{i=1}^{n+1}) \tag{6}$$

As a result, m enhancement nodes are updated according to the arbitrarily generated weights X_{ei}, α_{ei}, $i = 1,...,m$.

$$E_{en_m} \triangleq [\epsilon(S_{n+1}X_{en_1}+\alpha_{en_1}),\ldots,\epsilon(S_{n+1}X_{en_m}+\alpha_{en_m})] \tag{7}$$

Second, if the $(m+1)^{th}$ group of enhancement nodes $E^{(m+1)}$ are incrementally added as follows:

$$E_{m+1} \triangleq [\epsilon(S^{n+1}X_{E_{m+1}}+\alpha_{E_{m+1}})] \tag{8}$$

Our method inherits the advantage of fast incremental learning specifically in a cascade way as follows:

$$C_n^{m+1} \triangleq [S^n|E^m] \tag{9}$$

$$C_{n+1}^{m+1} \triangleq [C_n^m[S_{n+1}|E_{en_m}|E_{m+1}]] \tag{10}$$

To find the pseudo-inverse the representation of proposed CIL model for the output segmented vessels O, following formulation is used:

$$(C_{n+1}^{m+1})^+ = \begin{bmatrix} (C_n^m)^+ - PQ^T \\ Q^T \end{bmatrix} \tag{11}$$

$$X_{n+1}^{m+1} = \begin{bmatrix} X_n^m - PQ^TO \\ Q^TO \end{bmatrix} \tag{12}$$

where

$$\therefore P = (C_n^m)^+[S_{n+1}|E_{en_m}|E_{m+1}]$$

$$\therefore R = [S_{n+1}|E_{en_m}|E_{m+1}] - C_n^mP$$

$$\therefore Q^T = \begin{cases} (R)^+ & \text{If } R \neq 0 \\ (1+P^TP)^{-1}P^T(C_n^m)^+, & R = 0 \end{cases}$$

B. Tree Representation Based on Anatomical Variations of Liver Vasculature

To describe anatomical variations of hepatic artery [39] for this research, we have used the most common 10 types of hepatic artery variations by Michel's classification [20] as it provides the well-established anatomic approach. Among Michel's types, the first one represents the conventional anatomy and II to X for other nine variants. Type I anatomy (or conventional type) is most popular about general structure of HA contains 55 to 76% of the patients depending on the study. The common hepatic artery (CPA), starting from the celiac artery (CA) splits into the right hepatic artery (RHA) and left hepatic artery (LHA) followed by the proper hepatic artery. For any variant not described in types I-X is denoted as outlier and described in type XI but not mentioned in the table of Michel's 10 types. XIth category contains the variant not belong to any type of I-X categories. However, as anatomical variations may occur due to genetic aberrations in the embryonic period, no detailed classification can cover all types [40]. As it depends upon the study that how many patients fall in XIth category [41]. In case of our study, we have found almost 25 cases fall under X1th category. The precise knowledge of the most common and rare variations that produce different technical difficulties, or challenges, is essential to surgeons in order to avoid damage and vascular surgical complications. For rare anomalies, cases with the outliers the surgeons manually examine the hepatic variant

Authorized licensed use limited to: National Cheng Kung Univ.. Downloaded on July 20,2021 at 04:15:33 UTC from IEEE Xplore. Restrictions apply.

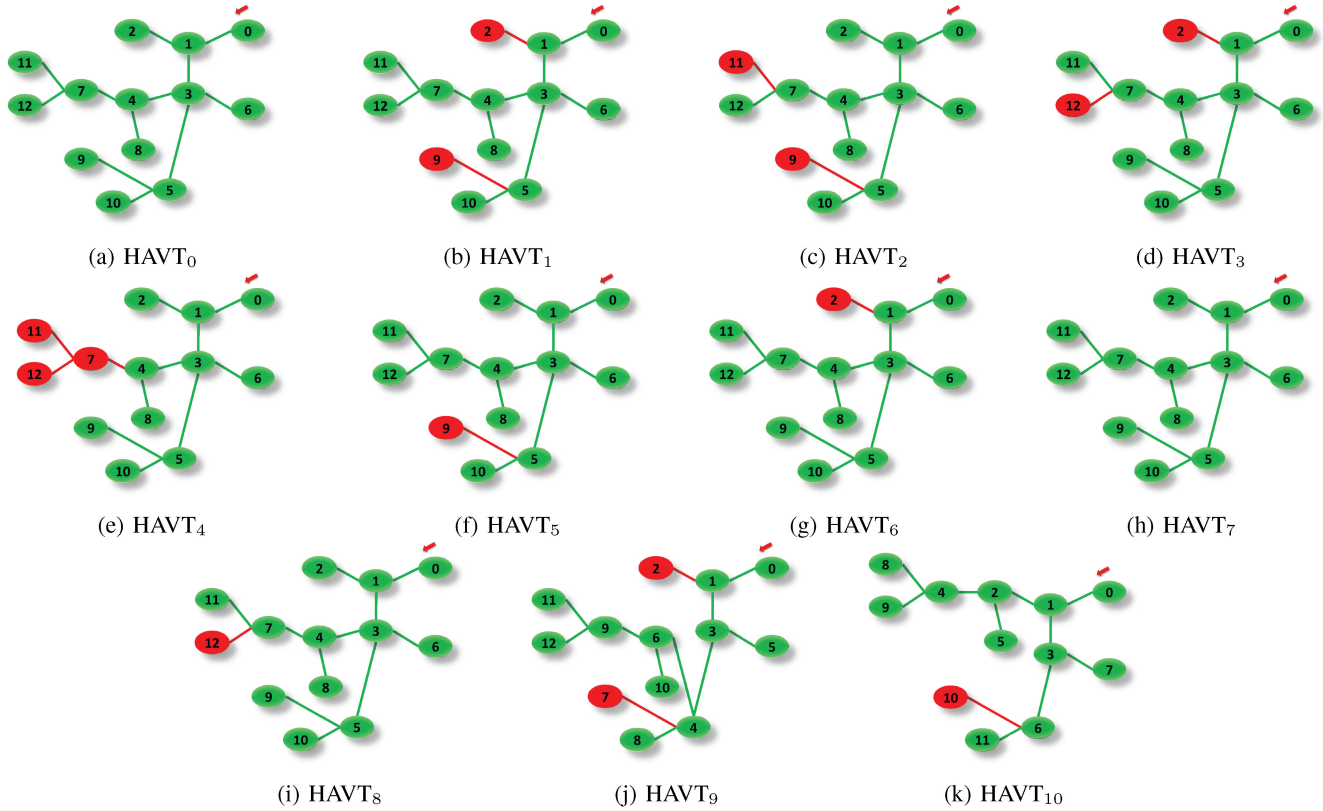

(a) $HAVT_0$ (b) $HAVT_1$ (c) $HAVT_2$ (d) $HAVT_3$

(e) $HAVT_4$ (f) $HAVT_5$ (g) $HAVT_6$ (h) $HAVT_7$

(i) $HAVT_8$ (j) $HAVT_9$ (k) $HAVT_{10}$

Fig. 5. Tagged vessels structure in the form of ternary tree topologies representation based on anatomical variations of hepatic artery of liver. (a) First one represents the general type of all variants while (b-k) represents the 10 variants of hepatic artery. A node represents bifurcate/trifurcate of vessels structure and edge represents the connection between the vessels. Deleted nodes are represented by red lines and green lines represent the nodes included in the variants.

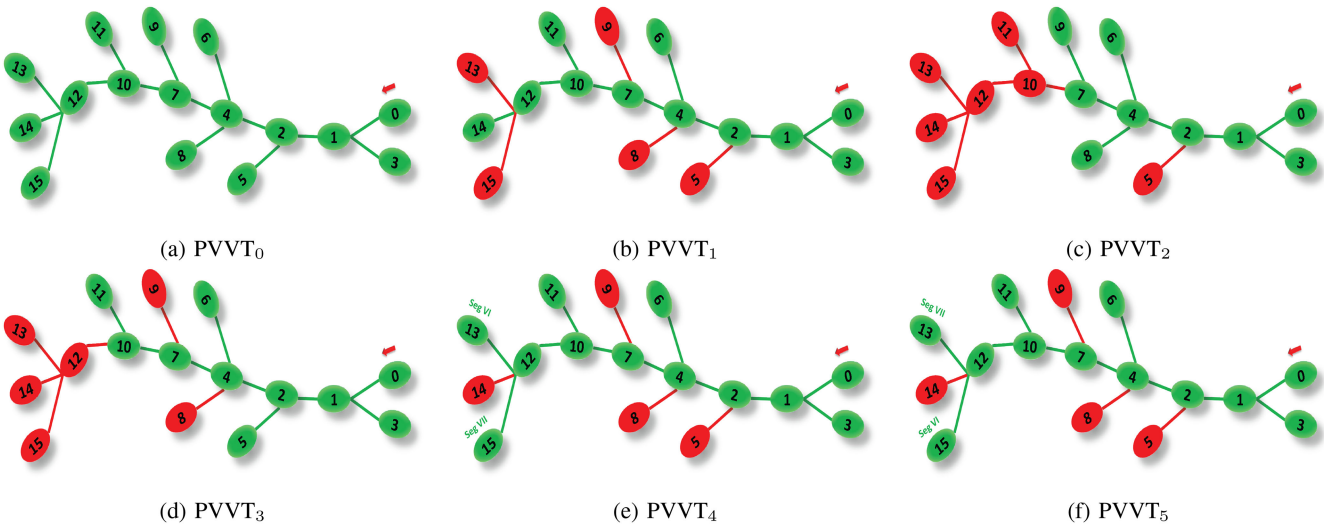

(a) $PVVT_0$ (b) $PVVT_1$ (c) $PVVT_2$

(d) $PVVT_3$ (e) $PVVT_4$ (f) $PVVT_5$

Fig. 6. Tagged vessels structure in the form of ternary tree topology based on anatomical variations for portal vein of liver. (a) First one represents the general type of all variants while (b-f) represents the 5 variants of tagged portal vein trees.

and found that case manually in available donors of that XI^{th} types.

The possible variants of hepatic artery and portal vein for tree representations are illustrated in Fig. 5 and Fig. 6. Based on the abovementioned hepatic artery and portal veins variants, we have mapped the possible combination of liver vasculature segmented using CIL from CTA volume with their respective tree representation.

Authorized licensed use limited to: National Cheng Kung Univ.. Downloaded on July 20,2021 at 04:15:33 UTC from IEEE Xplore. Restrictions apply.

Algorithm 1: Tree-Based Living Donor-Recipient (LDR) Liver Pair Matching.

Require: Recipient_tree(PVT,HAT),
Donor_tree_variant(PVTV$_{i\to n}$, HATV$_{i\to n}$).
ensure Matched_LDR_Liver().
PVTV $\leftarrow$ [PVTV$_1$, PVTV$_2$,..., PVTV$_n$];
HATV $\leftarrow$ [HATV$_1$, HATV$_2$,..., HATV$_n$];
for i=0; i $\leq$ n || EndOfTree**do**
Level_Based_Tagging$_{level=i\to n}$(PVT,PVTV$_{i\to n}$, HAT,HATV$_{i\to n}$);
end for
For k=1; PVTV $_{k\to n}$, PVTV$_{k\to n}$ ||$\leq$ n
Compare_Tree_Geometry[Recipient_tree(PVT,HAT), Donor_tree_variant(PVTV$_{k\to n}$,HATV$_{k\to n}$)];
Portal_InOrder_Traversal(PVT, PVTV$_{k\to n}$);
P_LeftSubTree();
P_MiddleSubTree();
P_RightSubTree();
Hepatic_InOrder_Traversal(HAT, HATV$_{k\to n}$);
H_LeftSubTree();
H_MiddleSubTree();
H_RightSubTree();
Calculate CAL Score(PVT,HAT);
if ((PVT==PVTV $_{k\to n}$)&&(HAT==HATV$_{k\to n}$))
return PVTV$_k$, HATV$_k$;
else
Move to next variant
EndFor

Similarly, main portal vein (MPV) splits into left and right portal veins i.e. LPVs and RPVs respectively. RPV further partitions into the right anterior portal vein (RAPV) and right posterior portal vein (RPPV) which additionally subdivides segmental branches into superior and inferior parts. Liver segments II, III, and IV take blood supply from LPV trunk. Cheng *et al.* [39] described types I to IV portal vein anatomical variants while Nakamura *et al.* [42] classified portal veins into five variants, this research is based on these two well-known hepatic and portal vein classifications.

C. Tree Matching Based on Geometrically Varied Liver Vasculature Using Ternary Tree

Based on the ternary tree structure, we have proposed Algorithm 1 for comparing LDR liver vessels. Compared with the related work such as [34], [43], our approach tags the vessels structure in the form of ternary tree topologies to deliver a possible variation of hepatic and portal vessels structures. The tagging process follows in-order tree traversing and generates digital strings of variants. A matching process based on in-order digital string is introduced in this study. For this we have defined four parameters i.e. distinct nodes, most significant nodes, bifurcate and trifurcate points according to Table I. In-order digital representation is the simple digital strings of nodes enabled in a tree variant. Distinct nodes are combinations of deleted nodes which differentiate one variant from others and help to accelerate the matching process by eliminating those nodes during searching which are not parts of the digital string. Most significant nodes represent the points prior to distinct nodes. Bifurcate and trifurcate are the dividing points for vasculature tree into two and three children respectively.

Considering a starting process from the tree roots, edges and nodes of the donor's and recipient's trees are successively compared. To avoid redundant comparison, if a match between two trees is not found at the starting of in-order traverse (the leaf node) it will reject that specific variant and move to another alternative. This strategy makes the proposed approach a robust and cost effective solution.

IV. Evaluations and Discussions

A. Dataset Details

This work has been assessed on two datasets: (1) clinical dataset comprising of CTA volumes (axial type) of 1 K patients from a partner hospital in Shanghai China and (2) a publicly available SLIVER07[1] dataset. The dataset consists of total 20 training and 10 testing scans. For the clinical dataset, each CTA volume includes arterial, portal, venous, and equilibrium phases having approximately 56 images for each phase. The voxel spacing varies from (0.80 mm; 0.75 mm; 0.80 mm) to (0.90 mm; 1.0 mm; 0.90 mm) with a slice thickness of 3.5 mm. The manual labelling of the dataset for validation was done by an expert physician on 30 CTAs; in average, five to six hours was taken for each CTA to cover all possible variants of the hepatic artery and portal veins.

Out of the total 22400 images of clinical dataset, 12240 images were used for training. The training time of clinical datasets was approximately 350 seconds on a 2.70 GHz Intel Xeon E5-2680 CPU with GPU having NVIDIA GeForce GTX Titan. It took in average 20 seconds to segment the liver vessels from the CTA volume on a trained CIL network and around 10 seconds to find a match for an appropriate LDR pair.

B. Qualitative Evaluation

A matching evaluation process has been used for the LDR pair of the liver vasculatures. We exemplify an evaluation process where an input recipient's liver vasculature comprising of hepatic artery variant 8 (HAV$_8$) and portal vein variant 4 (PVV$_4$) was used as an input to search for appropriate donors.

1) Digital Strings Based Tree Variants Matching Results: Digital string formation procedure is described in Fig. 7. Our setup will match combination of (HAV$_8$ + PVV$_4$) with all the available possible donor's vasculatures having HAV (V$_1$ to V$_{10}$) and PVV (V$_1$ to V$_5$). During matching process, the recipient's combination matches its in-order digital string (2,1,11,7,4,8,3,9,5,10,6,0 + 6,4,7,11,10,13,12,15,2,1,3,0) with all other digital strings of HAV and PVV variants in an ascending strahler order.

For input recipient vasculature combination of (HAV$_8$ + PVV$_4$), the distinct nodes are 12 and 5, 8, 9, 14 for HAV

[1]Segmentation of the Liver 07: http://www.sliver07.org/

Authorized licensed use limited to: National Cheng Kung Univ.. Downloaded on July 20,2021 at 04:15:33 UTC from IEEE Xplore. Restrictions apply.

TABLE I
STATISTICS TO SHOW THE MATCHING PROCESS OF HEPATIC ARTERY AND PORTAL VEIN VARIANTS WITH RESPECT TO TERNARY TREE REPRESENTATION IN TERMS OF IN-ORDER DIGITAL STRINGS REPRESENTATION

Artery/Vein	Variants	In-Order Digital Representation	Distinct Nodes	Most Significant Node(s)	Bifurcate Node(s)
Hepatic Artery	HAV_1	1,11,7,12,4,8,3,5,10,6,0	2,10	1-no extension & 5-one extension	4(7,8),7(11,12)
	HAV_2	2,1,7,12,4,8,3,5,10,6,0	9,11	7-one extension & 5-one extension	1(2,3),4(7,8)
	HAV_3	1,11,7,12,4,8,3,9,5,10,6,0	2,12	1-no extension & 7-one extension	4(7,8),5(9,10)
	HAV_4	2,1,4,8,3,9,5,10,6,0	7,11,12	4-no extension	1(2,3),5(9,10)
	HAV_5	2,1,11,7,12,4,8,3,5,10,6,0	9	5-one extension	1(2,3),4(7,8),7(11,12)
	HAV_6	1,11,7,12,4,8,3,9,5,10,6,0	2	1-no extension	4(7,8),5(9,10),7(11,12)
	HAV_7	2,1,11,7,12,4,8,3,9,5,10,6,0	-	No empty	1(2,3),4(7,8),5(9,10),7(11,12)
	HAV_8	2,1,11,7,4,8,3,9,5,10,6,0	12	7-one extension	1(2,3),4(7,8),5(9,10)
	HAV_9	1,11,9,12,6,10,4,8,3,5,0	2,7	1-no extension & 4-one extension	3(4,5),4(6,8),6(9,10),9(11,12)
	HAV_{10}	8,4,9,2,5,1,6,11,3,7,0	10	6-one extension	1(2,3),2(4,5),3(6,7),4(8,9)
Portal Vein	PVV_1	6,4,7,11,10,12,14,2,1,3,0	9,13,15,8,5	12-only one child	1(2,3),10(11,12)
	PVV_2	6,4,9,7,8,2,1,3,0	5,10,12,13,14,15	7-No child	1(2,3),4(6,8)
	PVV_3	6,4,7,11,10,2,5,1,3,0	8,9,12,13,14,15	10-No child	1(2,3),2(4,5),4(6,7)
	PVV_4	6,4,7,11,10,13,12,15,2,1,3,0	5,8,9,14	13-Seg VI, 15-Seg VII	1(2,3),10(11,12),12(13,15)
	PVV_5	6,4,7,11,10,13,12,15,2,1,3,0	5,8,9,14	13-Seg VI, 15-Seg VI	1(2,3),10(11,12),12(13,15)

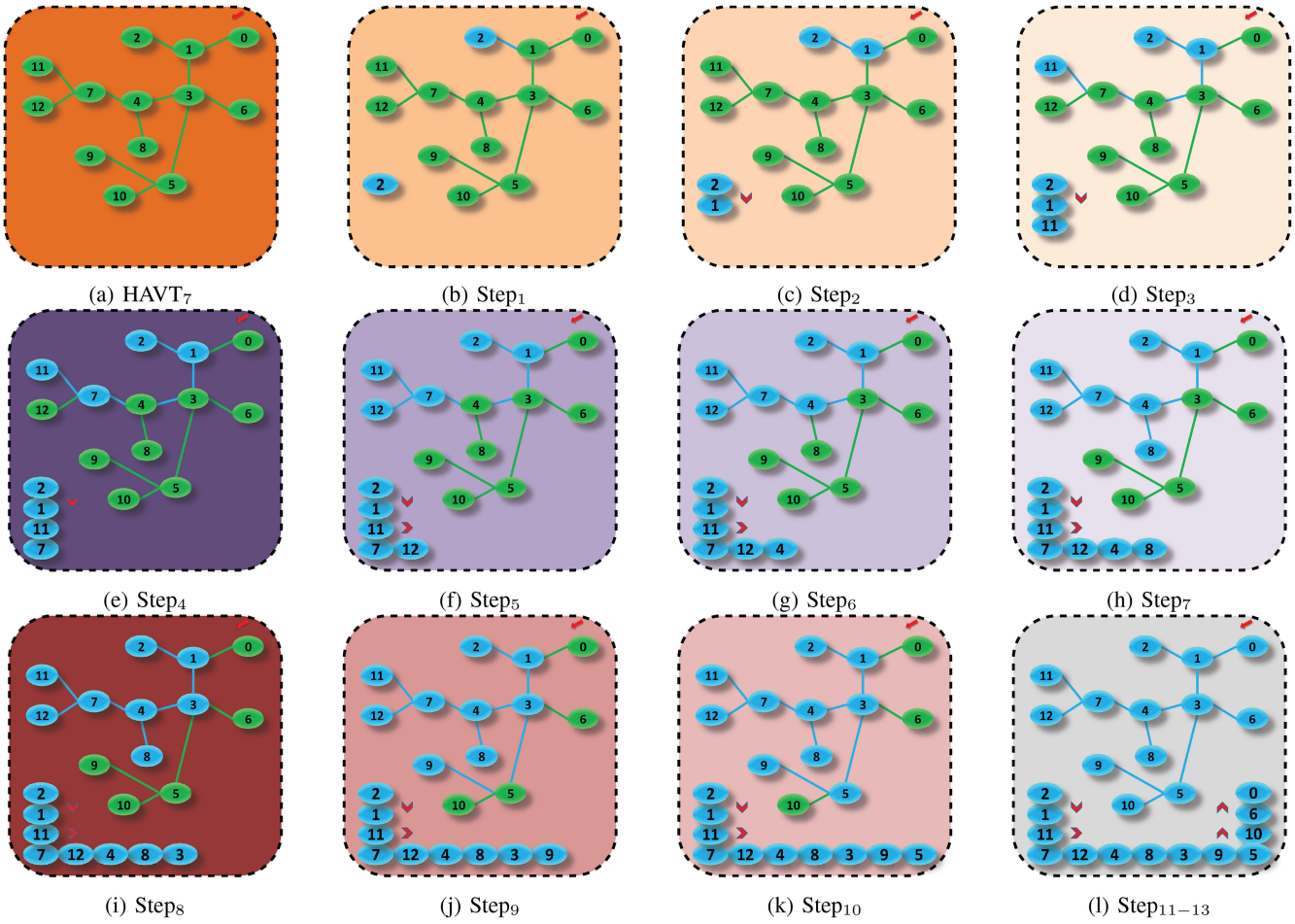

Fig. 7. First part (a) is showing candidate hepatic artery variant $HAVT_7$ while other parts (b to l) represents the process of stepwise workflow of digital string formation.

and PVV respectively. The distinct nodes are those which are not the part of required variants. Most significant node values represent the points prior to distinct nodes and include 7 and 12 for hepatic artery and portal vein variants, respectively. We have found three bifurcate points i.e., 1(2, 3), 4(7, 8), and 5 (9, 10) and one trifurcate point 3(4, 5, 6) for HAV while PVV include three bifurcate 1(2, 3), 10(11, 12), and 12(13, 15) points. Using the abovementioned four parameters (in-order of digital representation, distinct nodes, most significant nodes, bifurcate and trifurcate points), we have found an exact matching as shown

Authorized licensed use limited to: National Cheng Kung Univ.. Downloaded on July 20,2021 at 04:15:33 UTC from IEEE Xplore. Restrictions apply.

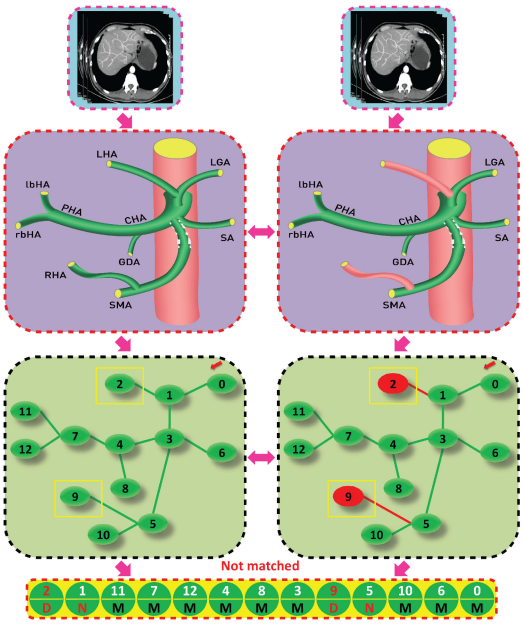

Fig. 8. Interactive visualization of liver vessels tree structure using in-order tree traversal with a novel concept of digital string as a robust guidance tool during intra-operative liver transplant. Where, liver recipient having (HAV_7+HAV_1 variants) topology is matched with its available donors in a reciprocal manner with notation M for successfully matched, N for unmatched and D for distinct nodes.

TABLE II
RESULTS OF OUR APPROACH FOR VARIOUS STRUCTURAL REPRESENTATION OF CIL NETWORK (NO. OF FEATURE NODES + NO. OF ENHANCEMENT NODES)

Dataset	No. of F.N	No. of E.N	Accuracy (%)	Training Time (s)	MTE (%)	ATE (%)
SLIVER07	50	100	98.43	78	3.48	3.98
	200	300	98.57	90	3.39	3.84
	300	500	98.68	120	3.20	3.54
	500	700	98.72	150	3.00	3.40
	700	1000	98.79	170	2.90	3.20
	900	1200	98.83	200	2.76	3.05
	1000	1500	98.89	250	2.75	3.02
Clinical	500	800	98.12	170	3.30	3.90
	700	1100	98.30	190	3.21	3.80
	900	1500	98.55	210	3.15	3.60
	1100	2400	98.67	250	3.05	3.32
	1500	2500	98.79	280	2.80	3.10
	2000	2900	98.89	300	2.70	3.02
	2500	3000	98.90	350	2.67	3.00

in Fig. 8. The obtained matching results are verified by expert surgeons with the help of manually labeled GT of well-known hepatic artery and portal vein variants.

C. Quantitative Analysis

The liver vessels segmentation results obtained based on our CIL are validated quantitatively using four metrics i.e. accuracy (%), training time (seconds), maximum testing error (MTE (%)) and average testing error (ATE (%)) on SLIVER07 as well as clinical datasets.

1) Vessels Segmentation Results: CIL network structure used for SLIVER07 dataset is discussed in Table II. The first column shows the number of feature nodes (50-1000) and second column is representing the number of enhancement nodes (100-1500) with learning rate 0.04 and the weight decay of 0.001. The numbers of trails are almost 100-120 times. As expected, by increasing the number of feature and enhancement nodes we have achieved better results i.e. less MTE (2.75%) and ATE errors (3.02%) and higher accuracy up-to 98.89% but with increased training time i.e. 250 seconds.

For clinical dataset we have utilized feature nodes up-to (500-2500) and number of enhancement nodes include values in the range of (800-3000) with learning rate 0.04 and the weight decay of 0.001. The experiments for clinical dataset include up-to 2000 trails. The proposed algorithm works well with our private data for liver vessels segmentation as the training data include diversity and consistent to SLIVER07 results. Although with increasing number of feature and enhancement nodes, training time increases (170 s to 350 s) but it delivers satisfied results in the form of lowering MTE (3.30% to 2.70%) and ATE (3.90% to 3.00%) errors and alleviating accuracy up-to (98. 90%) for segmentation. Our proposed model enhances accuracy level for segmenting liver vessels in terms of increased success rate to maximize the availability of an appropriate LDR match.

2) Tree Matching Results: To demonstrate accuracy of ternary tree matching from a different point of view, we have conducted experiments to reveal the success and failure rate [45] for matching a candidate recipient liver variant with its potential possible donor liver vasculatures variants. Following four metrics i.e. failure rate, partially failure rate, success rate and partially success rate are used to carry out testing trials. For quantitative analysis of the proposed approach, we have measured the similarity of two vascular trees in terms of success and failure rates for the matching process. In our setup, success rate is defined as number of successfully matched LDR liver vessels pairs to the total number of available pairs Failure rate is a percentage measured as total number of unmatched LDR liver vessels pairs to the total number of available LDR liver vessels pairs. Statistical results using the clinical dataset for success and failure rates of proposed approach are described in Table III. Where the HAV_1 and PVV_1 have shown higher success and lower failure rates, as these variants are the most common among population hence maximum match found for these variants among the given testing trails. Fig. 9 and Fig. 10 shows the process of matching between two liver variants, where black and yellow regions represent mismatched nodes, blue region represent distinct/disabled nodes, and other regions represent successfully matched nodes.

D. Comparison With State-of-The-Art Vessel Segmentation Methods

We have compared results with three state-of-the-art approaches i.e. Jin *et al.* [30], Huang *et al.* [29] and He *et al.* [44] in terms of network structure parameters i.e. number of neurons (millions), number of parameters (millions), training time (minutes), and accuracy (%). Table IV and Fig. 11 shows that we have achieved satisfactory results which are comparable to that of the Jin *et al.* [30] in terms of training time and accuracy.

Authorized licensed use limited to: National Cheng Kung Univ.. Downloaded on July 20,2021 at 04:15:33 UTC from IEEE Xplore. Restrictions apply.

TABLE III
QUANTITATIVE RESULTS TO EXPRESSES SUCCESS RATE, FAILURE RATE, PARTIALLY SUCCESS RATE AND PARTIALLY FAILURE RATE OF THE PROPOSED APPROACH FOR TREE MATCHING

Artery/Vein Structure	Hepatic/Portal Variants	Success rate (%)	Failure rate (%)	P_Success rate (%)	P_Failure rate (%)	Ratio (%) (Succ : Fail)
Hepatic Artery Variants	HAV_1	80.110	2.033	2.667	35.246	80 : 2
	HAV_2	78.916	1.449	5.349	16.355	78 : 1
	HAV_3	83.826	2.569	5.064	15.423	83 : 2
	HAV_4	74.345	4.369	2.063	20.117	74 : 4
	HAV_5	69.216	4.778	5.445	22.413	69 : 4
	HAV_6	77.313	3.188	2.113	18.345	77 : 3
	HAV_7	73.219	2.345	2.114	23.456	73 : 2
	HAV_8	69.003	1.005	2.666	28.364	69 : 1
	HAV_9	70.450	5.673	4.366	21.311	70 : 5
	HAV_{10}	65.128	2.113	3.234	15.336	65 : 2
Portal Vein Variants	PVV_1	84.220	1.205	3.557	12.346	84 : 1
	PVV_2	78.342	2.113	5.644	15.345	78 : 2
	PVV_3	73.169	2.935	4.344	21.445	73 : 2
	PVV_4	82.119	4.342	4.341	20.450	82 : 4
	PVV_5	64.332	2.113	4.311	30.110	64 : 2

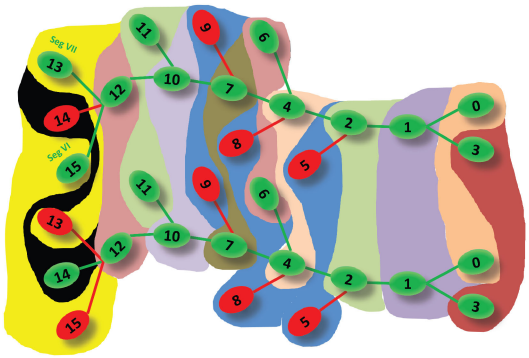

Fig. 9. Visualization of unsuccessful liver donor-recipient pair matching case. Where, black and yellow regions are showing the points of unmatched tree nodes for the respective recipient with its available living donors while other regions are showing the matching process. The illustrated demonstration will prove to be a quick assessment for the selection of appropriate candidate during pre-operative analysis in liver transplant.

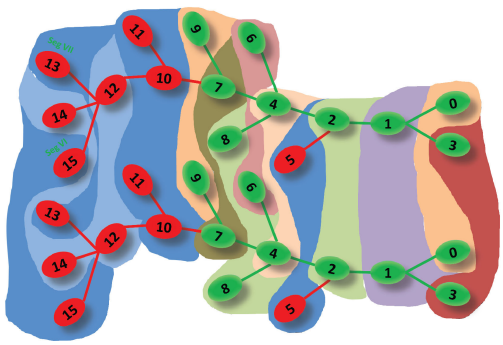

Fig. 10. Visual representation of successful liver donor-recipient pair matching case where the LDR pair is matched node by node.

However, our method has achieved better results compared to Huang *et al.* [29] in terms of training time and high accuracy of vessels segmentation even with usage of fewer number of neurons and parameters.

1) Outcomes of CIL's Segmentation After Retraining: In liver transplantation problem to maintain diversity of vessels structure, our constructed model is adaptive for new data.

TABLE IV
SEGMENTATION PERFORMANCE OF PROPOSED METHOD WITH THREE STATE-OF-THE-ART APPROACHES IN TERMS OF NO. OF NEURONS (NO. OF NEO), NO. OF PARAMETERS (NO. OF PARA), TRAINING TIME, AND ACCURACY ON CLINICAL DATASET IS PRESENTED IN FIRST ROW. THE SECOND ROW PRESENTS STATISTICS IN TERMS OF ADDITIONAL FEATURE NODE (ADD F.N), ENHANCEMENT NODES (ADD E.N), TRAINING TIME (ADD T.T) AND ACCURACY WHEN THERE IS REQUIREMENT TO ACCOMMODATE NEW INPUT

Metrics	Jin et al. [30]	Huang et al. [29]	He et al. [44]	CIL
No. of Neo	18.35	24.45	18.88	10.80
No. of Para	15.31	30.57	24.75	13.29
Training Time	6.33	10.83	10.66	5.83
Accuracy	94.75	90.01	95.90	98.90
Add F.N	500-550	650-700	850-900	950-1000
Add E.N	1000-1200	1500-1700	1800-2000	2300-2500
Add T.T	18.29	24.37	36.44	32.01
Accuracy	98.47	96.13	97.05	98.97

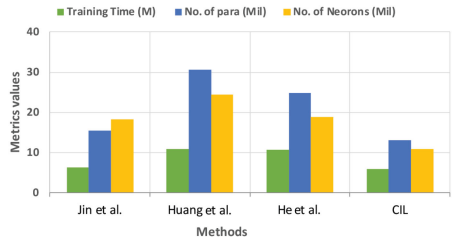

Fig. 11. Graphical comparison of proposed method with three state-of-the-art segmentation techniques [29], [30], [44].

We have demonstrated the achievement of better segmentation results by introducing CIL model for newly added features/enhancement nodes with respect to additional training time and related accuracy. The analysis of additional nodes and respective decreased training time as compare to state-of-the-art Jin *et al.* [30], Huang *et al.* [29] and He *et al.* [44] shows that our proposed model perform better when there is need to update the input data at runtime without need of training the whole system.

2) Comparison With State-of-The-Art Tree Matching Methods: we have presented an extensive analysis on comparing proposed method variants and existing tree

Authorized licensed use limited to: National Cheng Kung Univ.. Downloaded on July 20,2021 at 04:15:33 UTC from IEEE Xplore. Restrictions apply.

TABLE V
QUANTITATIVE RESULTS TO DEMONSTRATE THE VARIOUS STATE-OF-THE-ART TREE MATCHING METHODS ALONG WITH PROPOSED METHOD (P.M) SEGMENTATION RESULTS

	Input samples w.r.t 1k			Input samples w.r.t 2k		
Method	Success Rate	Failure Rate	Classification Error	Success Rate	Failure Rate	Classification Error
Yan et al. [1]	89.11	9.23	0.35	91.12	8.21	0.33
O'Donnell et al. [22]	80.23	15.44	0.56	82.11	13.23	0.52
Charnoz et al. [43]	84.11	12.33	0.46	86.95	10.43	0.41
P.M with CIL UpdatedSeg	96.97	2.31	0.21	98.11	1.50	0.15

matching approaches in terms of success and failure rates with classification error in Table V. Our method achieved higher success rate of 98.11 % and lowered classification error of up to 0.15 when we obtained segmentation results after CIL with new data adoption. The newly added input helps to maximize the chance of finding an appropriate match for the candidate recipient against the possible donor variants, which adds up to our accuracy level in terms of increasing the success rate of our approach as compared to state-of-the-art models.

E. Discussion on Tree Matching Process Based on CAL Score and Classification Error

We have performed the task of finding an appropriate LDR liver pair as tree modelling problem, with possible hepatic artery and portal vein variants. For experimental analysis, we have calculated the success and failure rates based on CAL (connectivity, area, and length of vessels branches) score for each variant to compare the topological variations between two liver variants at concrete level. With the human quality observation in delineating the vessel trees, CAL score is considered to be a well matching metric [46]. The CAL score is known as a substitute evaluation metric of vessel segmentation. The CAL score comprises three components: L demonstrates the length of the extracted vessel; A represents the overlapping area between segmented image and ground-truth; and C refers to the vessel connectivity. To conclude, it is represented by a single CAL score, which is calculated by the production of abovementioned three components. The range of all these values is within the range of $[0, 1]$ where higher value means the better one. Connectivity for a variant is described by angle (θ) between two branches of vessel at bifurcation/trifurcation point, area of a vessel is the diameter of a specific branch in mm, and length of vessel branch is the distance measured in mm between two bifurcation/trifurcation points. For an exact matching between two variants, the angles, diameter and length between two bifurcate points should be similar. The comparing process of in-order ternary tree traversing match the recipient CAL score with the all possible donor's CAL scores.

With the human quality observation in delineating the vessel trees, CAL score is considered to be a well matching metric for more details see Table VI. The higher value of radius means the matching processes is now comparing the critical vessels. The angle (θ) determines the shape of variant in a way that if two variants have a bifurcation point at the same length but having varied θ means these are two different variants.

To verify the tree matching process, we have compared the results of successfully matched (success rate) variants to the ground truth. We have generated their classification errors (η) by dividing the number of mismatched variants (failure rates) into the total number of available variants as follows: $\eta = \frac{|V_e|}{|V|}$, where $|V_e|$ is the total number of mismatched variants and $|V|$ denotes the total number of available variants. The matches which is having labels as partially success and partially failure rates are not counted in both $|V|$ and $|V_e|$ for fairness because these variants are the results of mismatch. Fig. 12 shows the comparison process of classification error of proposed method with the state-of-the-art liver vessels tree matching approaches. our model has achieved improved tree matching results having lesser classification error up to 0.15 with 1200 input images which shows its superiority on the existing method.

TABLE VI
CAL SCORES FOR THE HEPATIC ARTERY AND PORTAL VEIN VARIANTS

Variant Type	C	A	L	CAL
HAV_1	0.9831	0.8673	0.7765	0.6620
HAV_2	0.9854	0.7895	0.6755	0.5255
HAV_3	0.9874	0.7654	0.8887	0.6716
HAV_4	0.9887	0.8658	0.7876	0.6741
HAV_5	0.9844	0.7554	0.7654	0.5691
HAV_6	0.9823	0.9987	0.8776	0.8609
HAV_7	0.9844	0.8865	0.7885	0.6881
HAV_8	0.9866	0.8874	0.6654	0.5825
HAV_9	0.9788	0.6654	0.7554	0.4919
HAV_{10}	0.9766	0.8833	0.8733	0.7533
PVV_1	0.9866	0.7763	0.9876	0.7564
PVV_2	0.9788	0.7543	0.6689	0.4938
PVV_3	0.9766	0.8223	0.9987	0.8020
PVV_4	0.9886	0.8774	0.8443	0.7323
PVV_5	0.9976	0.8654	0.7654	0.6607
PVV_6	0.9965	0.5853	0.8761	0.7467

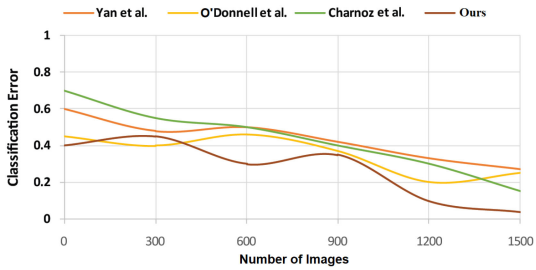

Fig. 12. Classification error based graphical comparison of proposed method with three state-of-the-art tree matching approaches [1], [22], [43].

V. CONCLUSION

We presented a new method for living donor-recipient liver pair matching. In our approach, liver vessel systems were

Authorized licensed use limited to: National Cheng Kung Univ.. Downloaded on July 20,2021 at 04:15:33 UTC from IEEE Xplore. Restrictions apply.

segmented from CTA volumes using the incremental concept of cascade feature mapping nodes as an optimal alternative for adapting the new training data. The segmented vessels were then mapped to tree representation using ternary tree data structure based on (Michel's X types) hepatic artery and portal vein variants. Matching process efficiently employed ternary tree in-order traversing to find an appropriate match between given recipient against its possible donor variants. Clinically such solutions will provide surgeons a comprehensive guidance for pre-operative evaluation of the liver vascular system to understand the variations of living donor-recipient (LDR) vascular anatomy. Quantitative assessment for similarity measure of compared vascular trees was carried out using Strahler ordering metric. Obtained results compared to the tagged variants of liver vessels structures demonstrated the effectiveness of the proposed approach.

References

[1] Z. Yan, F. Chen, and D. Kong, "Liver venous tree separation via twin-line RANSAC and Murray's law," *IEEE Trans. Med. Imag.*, vol. 36, no. 9, pp. 1887–1900, Sep. 2017.

[2] G. Li *et al.*, "Automatic liver segmentation based on shape constraints and deformable graph cut in CT images," *IEEE Trans. Image Process.*, vol. 24, no. 12, pp. 5315–5329, Dec. 2015.

[3] K. Drechsler *et al.*, "Semi-automatic anatomical tree matching for landmark-based elastic registration of liver volumes," *J. Healthcare Eng.*, vol. 1, no. 1, pp. 1–24, 2010.

[4] X. Chen *et al.*, "Medical image segmentation by combining graph cuts and oriented active appearance models," *IEEE Trans. Image Process.*, vol. 21, no. 4, pp. 2035–2046, Apr. 2012.

[5] G. Zhang *et al.*, "Generalized adaptive Gaussian Markov random field for x-ray luminescence computed tomography," *IEEE Trans. Biomed. Eng.*, vol. 65, no. 9, pp. 2130–2133, Sep. 2018.

[6] Y. Pei *et al.*, "Superimposition of cone-beam computed tomography images by joint embedding," *IEEE Trans. Biomed. Eng.*, vol. 64, no. 6, pp. 1218–1227, Jun. 2017.

[7] P. Lu *et al.*, "Highly accurate facial nerve segmentation refinement from CBCT/CT imaging using a super-resolution classification approach," *IEEE Trans. Biomed. Eng.*, vol. 65, no. 1, pp. 178–188, Jan. 2018.

[8] V. Cherukuri *et al.*, "Learning based segmentation of CT brain images: Application to postoperative hydrocephalic scans," *IEEE Trans. Biomed. Eng.*, vol. 65, no. 8, pp. 1871–1884, Aug. 2018.

[9] M. N. Cheema *et al.*, "Liver extraction using residual convolution neural networks from low-dose CT images," *IEEE Trans. Biomed. Eng.*, vol. 66, no. 9, pp. 2641–2650, Sep. 2019.

[10] A. K. Singh *et al.*, "Imaging of preoperative liver transplantation in adults: What radiologists should know," *Radiographics*, vol. 31, no. 4, pp. 1017–1030, 2011.

[11] O. A. Catalano *et al.*, "Vascular and biliary variants in the liver: Implications for liver surgery," *Radiographics*, vol. 28, no. 2, pp. 359–378, 2008.

[12] S. Moriconi *et al.*, "Inference of cerebrovascular topology with geodesic minimum spanning trees," *IEEE Trans. Med. Imag.*, vol. 38, no. 1, pp. 225–239, Jan. 2019.

[13] A. Farag *et al.*, "A bottom-up approach for pancreas segmentation using cascaded superpixels and (deep) image patch labeling," *IEEE Trans. Image Process.*, vol. 26, no. 1, pp. 386–399, Jan. 2017.

[14] Ö. Çiçek *et al.*, "3D U-net: Learning dense volumetric segmentation from sparse annotation," in *Proc. MICCAI*, 2016, pp. 424–432.

[15] Y. Cheng *et al.*, "Accurate vessel segmentation with constrained b-snake," *IEEE Trans. Image Process.*, vol. 24, no. 8, pp. 2440–2455, Aug. 2015.

[16] C. L. P. Chen and Z. Liu, "Broad learning system: An effective and efficient incremental learning system without the need for deep architecture," *IEEE Trans. Neural Netw. Learn. Syst.*, vol. 29, no. 1, pp. 10–24, Jan. 2018.

[17] D. Barbosa *et al.*, "B-spline explicit active surfaces: An efficient framework for real-time 3-D region-based segmentation," *IEEE Trans. Image Process.*, vol. 21, no. 1, pp. 241–251, Jan. 2012.

[18] S. Feng and C. L. P. Chen, "Fuzzy broad learning system: A novel neuro-fuzzy model for regression and classification," *IEEE Trans. Cybern.*, vol. 50, no. 2, pp. 414–424, Feb. 2020.

[19] F. Ritter *et al.*, "Real-time illustration of vascular structures," *IEEE Trans. Visual. Comput. Graph.*, vol. 12, no. 5, pp. 877–884, Sep./Oct. 2006.

[20] N. A. Michels, "Newer anatomy of the liver and its variant blood supply and collateral circulation," *Amer. J. Surg.*, vol. 112, no. 3, pp. 337–347, 1966.

[21] C. L. P. Chen, Z. Liu, and S. Feng, "Universal approximation capability of broad learning system and its structural variations," *IEEE Trans. Neural Netw. Learn. Syst.*, vol. 30, no. 4, pp. 1191–1204, Apr. 2019.

[22] T. O'Donnell *et al.*, "Venous tree separation in the liver: Graph partitioning using a non-ising model," in *Proc. Int. Conf. Inf. Process. Med. Imag. (IPMI)*, 2011, pp. 197–207.

[23] S. R. Aylward *et al.*, "Registration and analysis of vascular images," *IJCV*, vol. 55, pp. 123–138, 2003.

[24] J. Prassni, T. Ropinski, and K. Hinrichs, "Uncertainty-aware guided volume segmentation," *IEEE Trans. Visual. Comput. Graph.*, vol. 16, no. 6, pp. 1358–1365, Nov./Dec. 2010.

[25] M. A. Rodriguez and P. Neubauer, "The graph traversal pattern," in *Proc. Graph Data Manage.: Techn. Appl.*, S. Sakr and E. Pardede, Eds. Hershey, PA: IGI Global, 2012, pp. 29–46.

[26] D. A. Oliveira, R. Q. Feitosa, and M. M. Correia, "Segmentation of liver, its vessels and lesions from ct images for surgical planning," *Biomed. Eng. Online*, vol. 10, no. 1, pp. 1–23, 2011.

[27] A. Nazir *et al.*, "SPST-CNN: Spatial pyramid based searching and tagging of liver's intraoperative live views via cnn for minimal invasive surgery," *J. Biomed. Informat.*, vol. 106, 2020, Art. no. 103430.

[28] A. Nazir *et al.*, "OFF-eNET: An optimally fused fully end-to-end network for automatic dense volumetric 3D intracranial blood vessels segmentation," *IEEE Trans. Image Process.*, vol. 29, no. 1, pp. 7192–7202, 2020.

[29] Q. Huang *et al.*, "Robust liver vessel extraction using 3D U-net with variant dice loss function," *Comput. Biol. Med.*, vol. 101, pp. 153–162, 2018.

[30] J. Jin, Z. Liu, and C. P. Chen, "Discriminative graph regularized broad learning system for image recognition," *Sci. China Inf. Sci.s*, vol. 61, no. 11, 2018, Art. no. 112209.

[31] M. Xu *et al.*, "Recurrent broad learning systems for time series prediction," *IEEE Trans. Cybern.*, vol. 50, no. 4, pp. 1405–1417, Apr. 2020.

[32] A. Myronenko and X. Song, "Point set registration: Coherent point drift," *IEEE Trans. Pattern Anal. Mach. Intell.*, vol. 32, no. 12, pp. 2262–2275, Dec. 2010.

[33] Z. Zhai *et al.*, "Pulmonary vessel tree matching for quantifying changes in vascular morphology," in *Proc. Med. Image Comput. Comput. Assisted Inter. (MICCAI)*, 2018, pp. 517–524.

[34] A. Charnoz *et al.*, "Design of robust vascular tree matching: Validation on liver," in *Proc. IPMI*. Springer, 2005, pp. 443–455.

[35] M. N. Cheema *et al.*, "Image-aligned dynamic liver reconstruction using intra-operative field of views for minimal invasive surgery," *IEEE Trans. Biomed. Eng.*, vol. 66, no. 8, pp. 2163–2173, Aug. 2019.

[36] L. O. Schwen and T. Preusser, "Analysis and algorithmic generation of hepatic vascular systems," *Int. J. Hepatol.*, vol. 2012, pp. 1–18, 2012.

[37] O. V. Ivashchenko *et al.*, "A workflow for automated segmentation of the liver surface, hepatic vasculature and biliary tree anatomy from multiphase MR images," *Magn. Reson. Imag.*, vol. 68, no. 1, pp. 53–65, 2020.

[38] X. Guo *et al.*, "A novel method to model hepatic vascular network using vessel segmentation, thinning, and completion," *Med. Biol. Eng. Comput.*, vol. 1, pp. 1–16, 2020.

[39] Y. Cheng *et al.*, "Variation of the intrahepatic portal vein; angiographic demonstration and application in living-related hepatic transplantation," *Transplant. Proc.*, vol. 28, no. 3, pp. 1–13, 1996.

[40] O. C. L. d. FONSECA-NETO *et al.*, "Anatomic variations of hepatic artery: A study in 479 liver transplantations," *ABCD. Arquivos Brasileiros de Cirurgia Digestiva* (São Paulo), vol. 30, no. 1, pp. 357–37, 2017.

[41] A. Durur Karakaya, M. Kantarci, and A. Yalcin, "A rare variation of hepatic arteries (michels type iv): MDCT angiographic findings," *Eurasian J. Med.*, vol. 41, no. 1, p. 63, 2009.

[42] T. Nakamura *et al.*, "Anatomical variations and surgical strategies in right lobe living donor liver transplantation: Lessons from 120 cases," *Transplantation*, vol. 73, no. 12, pp. 1896–1903, 2002.

[43] A. Charnoz *et al.*, "Tree matching applied to vascular system," in *Proc. Int. Workshop Graph-Based Representations Pattern Recognit.*, 2005, pp. 1–10.

[44] K. He *et al.*, "Deep residual learning for image recognition," in *Proc. Conf. IEEE Comput. Vis. Pattern Recognit.*, 2016, pp. 770–778.

[45] P. A. VanderLaan *et al.*, "Success and failure rates of tumor genotyping techniques in routine pathological samples with non-small-cell lung cancer," *Lung Cancer*, vol. 84, no. 1, pp. 39–44, 2014.

[46] B. Sheng *et al.*, "Retinal vessel segmentation using minimum spanning superpixel tree detector," *IEEE Trans. Cybern.*, vol. 49, no. 7, pp. 2707–2719, Jul. 2019.

Authorized licensed use limited to: National Cheng Kung Univ.. Downloaded on July 20,2021 at 04:15:33 UTC from IEEE Xplore. Restrictions apply.